Hindawi
Advances in Polymer Technology
Volume 2020, Article ID 8638076, 18 pages
https://doi.org/10.1155/2020/8638076

Research Article

Circumferential Expansion Property of Composite Wrapping System for Main Cable Protection of Suspension Bridge

Pengfei Cao,[1] Hai Fang,[1] Weiqing Liu,[1] Yong Zhuang,[2] Yuan Fang,[1] and Chenglin Li[1]

[1]*College of Civil Engineering, Nanjing Tech University, Nanjing 211816, China*
[2]*China Railway Major Bridge Reconnaissance & Design Institute Co. Ltd., Wuhan 430050, China*

Correspondence should be addressed to Hai Fang; fanghainjut@163.com

Received 6 October 2019; Accepted 2 April 2020; Published 5 May 2020

Guest Editor: Guangming Chen

A composite wrapping system for main cable protection of suspension bridges was designed by using prepreg fiber-reinforced composites and nitrile rubber. The circumferential expansion performance of the system was tested, and the curves of circumferential bearing capacity and radial displacement of the components were obtained. Failure modes of each group of components were compared and analyzed. The results show that most of the components are vertically fractured at the lap transition. The increase of the number of prepreg layers contributed the most to the circumferential bearing capacity of components, with a growth rate of 65.31%~109.01%. The increase of rubber belt layers had the most significant effect on the radial displacement of the components, with a growth rate of 7.06%~23.5%. In the initial stage of the test, the strain of each part of the component was smaller due to the compaction by the loading device, and the strain value of the component was generally linearly increased during the loading process, during which the strain of the overlap was the smallest. The calculated cross-sectional temperature deformation of the main cable is in good agreement with the experimental data. The application of the rubber belt increases the deformation of the main cable; therefore, the protection system for the main cable could have more deformation redundancy and delay the arrival of the ultimate strain of the outer prepreg wrap.

1. Introduction

With the rapid development of technology and the continuous improvement of material properties, modern suspension bridge [1], with its superior engineering structure [2], has become the preferred bridge type for the construction of long-distance bridges in the world. The main cable, sling, cable tower, floor system, and anchorage are five main structures of suspension bridges. According to different stiffness, suspension bridges are divided into two types [3], flexible suspension bridges and rigid suspension bridges. Flexible suspension bridge is a kind of low-load bridge with bridge decks directly laid on the suspended cable, which is mostly used for short-span bridges. Rigid suspension bridge is to lay the deck on the rigid beam; the rigid beam is suspended on the suspension cable through the suspension rod. Most modern suspension bridges are rigid suspension bridge, and Figure 1 is a general arrangement diagram of the second bridge of Yueyang Dongting Lake.

Among all structural components of a suspension bridge, main cables are the main supporting component of the entire bridge, and the service life of the main cable is accompanied by the full life cycle of the bridge. Corrosion of main cables on suspension bridge [4] is a nonnegligible problem on a worldwide basis. The corroded main cables are shown in Figure 2.

There have been some researches on the main cable protection system. The so-called Roebling system, created by John A Reobling [5] in the United States in the 1840s, is most widely used in traditional main cable protection systems. As shown in Figure 3, the sealing material is filled in the main cable wire and the putty is applied to the surface, then a wire of approximately 4 mm in diameter is wound along the main cable on the putty layer. Finally, the laminated coating [6] is homogeneously applied on the surface of the wound wire. The main purpose of this system is to seal the outer surface of the main cable to prevent and isolate the corrosion of the water, salt, and other corrosive

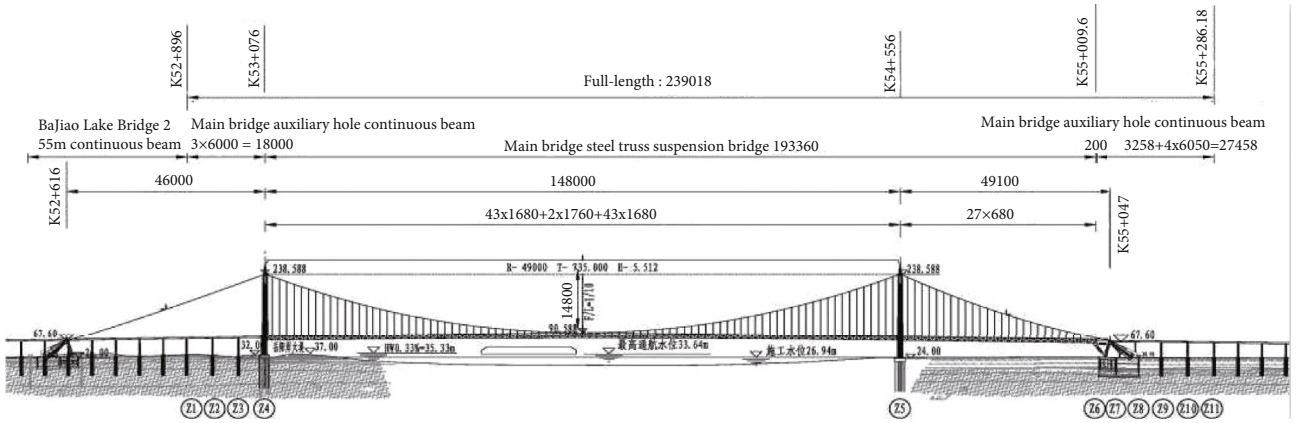

Figure 1: The general arrangement diagram of the second bridge of Yueyang Dongting Lake.

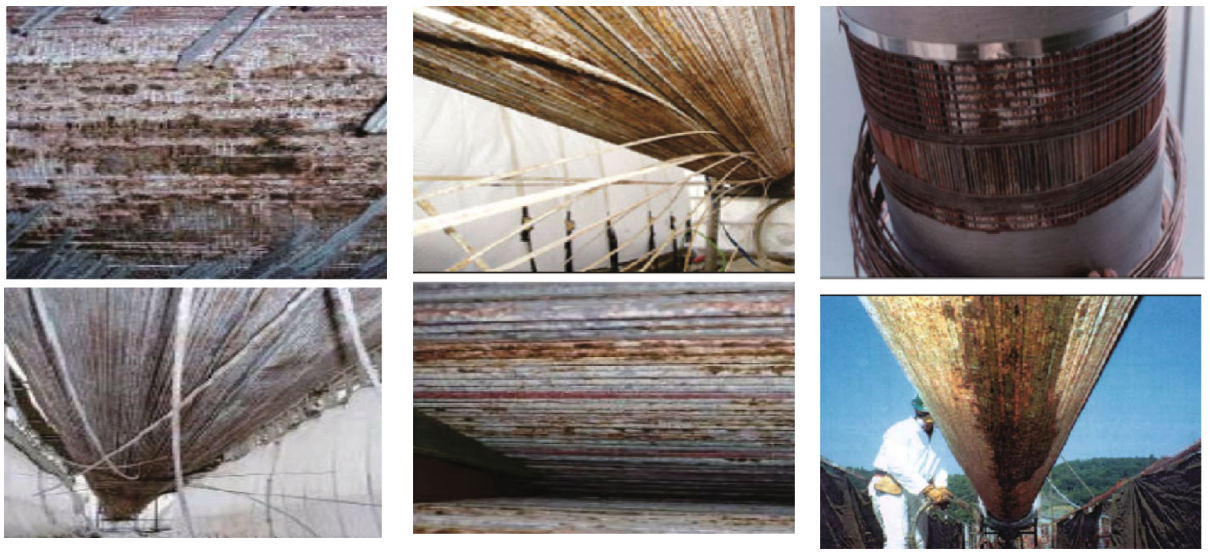

(a) (b) (c)

Figure 2: Corrosion of main cables on suspension bridge: (a) the Golden Gate Bridge, (b) Forth Road Bridge, and (c) Japan Dashima Bridge.

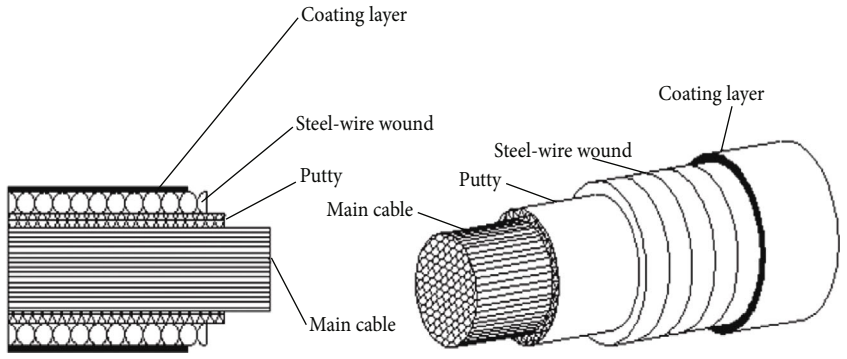

Figure 3: Schematic diagram of the Roebling system.

substances. However, the installation process of the system takes a long time from erection to completion; the aging and cracking phenomena will gradually appear in the coating layer. With the vibration of the suspension bridge, the length and the cross section of the main cable will be axially deformed at the same time. External coating is less elastic and easy to experience cracking, which leads to introduction of humid air.

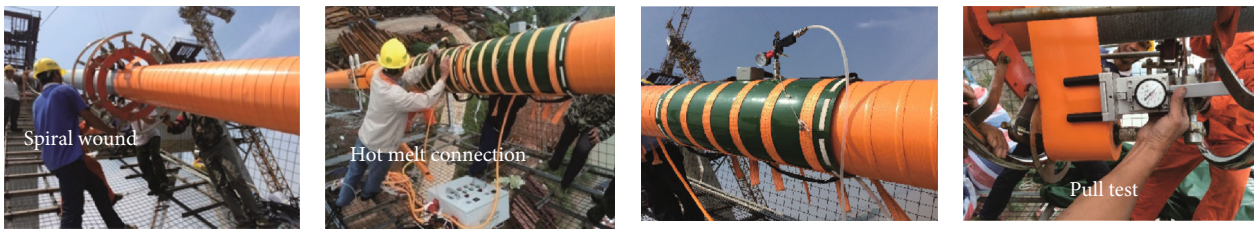

Figure 4: The construction process of winding and heating pressure vulcanization.

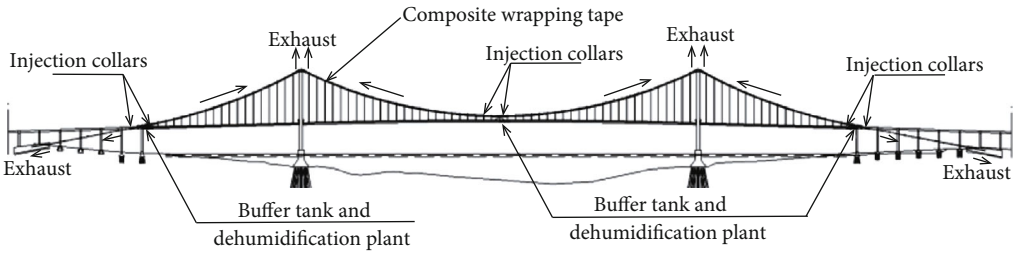

Figure 5: Principle of dehumidification and protection of the main cable.

Another protection system called synthetic sheath [7] was developed in the United States in the 1960s and 1970s to replace the Roebling system. The first layer of the protection system is wrapped with nylon belt on the main cable, then coated with binder on the nylon belt, finally wrapped with glass fiber polychloroprene rubber wrapping tape, polyester film, and polypropylene resin wrapping tape. Compared with the Roebling system, the construction process of the system is reduced. However, due to the instability of the early composite material performance, the technology is not mature enough. The effect of this protective system is not ideal, and it has not been widely used. In recent years, the fiber-reinforced composite wrapping tape structure was invented. It consists of unvulcanized chlorosulfonated polyethylene, fiber grid layout, and chlorosulfonated polyethylene. The matrix material of wrapping tape is chlorosulfonated polyethylene and the reinforcing material is fiber grid layout. This anticorrosion protection system of fiber-reinforced wrapping tape was first applied to Fengxi Bridge in Zhuzhou City, Hunan Province in China. Compared with the American Brown Wrap Belt, the elongation and tear strength have increased by 54% and 62%, respectively. Fiber-reinforced composite wrapping tape has excellent properties such as ageing resistance, easy maintenance, and replacement and gives full play to the remarkable advantages of lightweight, high strength, and corrosion resistance of fiber-reinforced composite materials. However, as shown in Figure 4, the biggest disadvantage of this system is that the installation process is cumbersome and complex.

Many examples have illustrated that the above two traditional protection systems for main cables cannot prevent corrosion basically, as such, a new system of corrosion management is necessary. A dehumidification system [8] was developed by Japan at the end of the 20th century. As shown in Figure 5, the main method of the system is to continuously fill the main cable with relatively dry air (humidity 40%-50%) and destroy the corrosion condition of the main cable so as to prevent the corrosion of the main cable steel wire. The cable dehumidification system was first applied to the Akashi Kaikyo Bridge [9], and it was understood that it had been performing adequately. Since then a small number of suspension bridges had been retrofitted with this system, and the majority of new bridges had been constructed with dehumidification installed as standard practice. The key to the dehumidification system was that the surface of the main cable could not be cracked; otherwise, it would seriously affect the dehumidification effect. On the other hand, the protection system needed to continuously provide dry air for the main cable throughout its life cycle, so the cost of the whole system was high.

There have been some researches on the influence of temperature field on the main cable. Taking Xihoumen Bridge as an example, it was found that under the effects of environmental factor, the cross-sectional temperature field of the main cable was obviously inhomogeneous. The temperature inside and outside the main cable had obvious phase difference, and the temperature amplitude was very different. For the suspension bridge with large-diameter main cable, even if the ambient temperature at night was relatively stable, there was a large difference between sectional weighted average temperature and superficial arithmetic mean temperature. The axial stress and average stress decrease with the increase of temperature, while the vertical moment increases with the increase of temperature. Under the effects of nonuniform temperature, the transverse moment of the main cable was produced, and the direction of the transverse moment pointed to the side with high temperature. So the main cable was deformed and damaged.

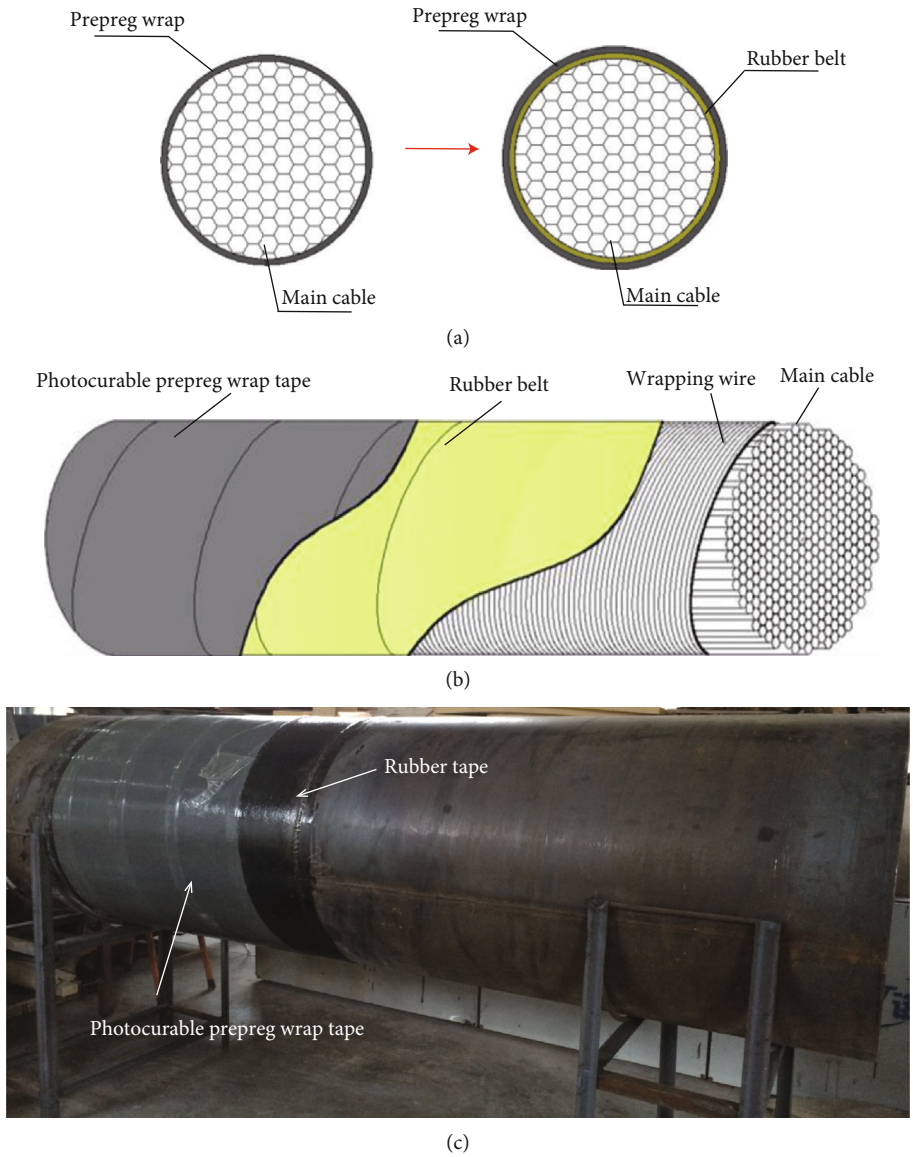

Figure 6: Schematic diagram of two samples: (a) section diagram of specimens, (b) structure diagram, and (c) actual diagram.

In view of the excellent protective performance and high corrosion resistance of FRP (Fiber-Reinforced Polymer) [10], sealing performance, and characteristics of reducing stress concentration of rubber material, this paper introduces the design and preparation process of the main cable protection system for the new suspension bridge using these two materials. This protection system needs to consider the influence of circumferential expansion of the main cable to protection system due to the external environment. This paper refers to the mechanical properties of FRP pipe under vertical compression of FRP-confined concrete members and uses this as a clue to study the mechanical properties of the main cable protection system under the action of internal circumferential expansion force, so as to guide the design of the new composite main cable protection system. Specimens were grouped, and circumferential expansion tests of specimens were carried out to study the different failure modes of specimens in each group. The circumferential bearing capacity-radial displacement curves and circumferential strain-radial displacement curves of components were obtained. The influences of the number of prepreg layers and rubber belt layers on the performance of the specimen were analyzed.

2. Experiment

2.1. Specimen Preparation. The sample materials were made of photocurable prepreg wrap tape and nitrile rubber belt. Specimens were divided into two types, as shown in Figure 6; one was a hoop specimen only made of photocurable prepreg wrap tape, and the other was a composite wrap tape made of photocurable prepreg wrap tape and nitrile rubber belt.

The first kind of specimens was divided into three groups; the first group was wrapped with 1-layer photocurable prepreg tape, the second group was wrapped with 2-layer

Table 1: Details of specimen.

Specimen	Layer of light-cured prepreg	Layer of elastic	Outer diameter (mm)	Inner diameter (mm)	Height (mm)	Number	FRP required (m^2)	Elastic layer required (m^2)
G-1-X	1	—	304	300	150	3	0.177	—
G-2-X	2	—	308	300	150	3	0.318	—
G-3-X	3	—	312	300	150	3	0.459	—
G-1-R-X	1	1	308	300	150	3	0.177	0.141
G-2-R-X	2	1	312	300	150	3	0.318	0.141
G-3-R-X	3	1	316	300	150	3	0.459	0.141
G-1-2R-1	1	2	312	300	150	1	0.177	0.282
G-2-2R-1	2	2	316	300	150	1	0.318	0.282
G-3-2R-1	3	2	318	300	150	1	0.459	0.282

G-1: a layer of photocurable prepreg FRP; R: a layer of elastic layer; 2R: two layers of elastic layer; X: the label of each component in a set of specimens.

photocurable prepreg tape, and the third group was wrapped with 3-layer photocurable prepreg tape.

The second kind of specimens was divided into four groups; the difference between the first three groups in the second kind and the first kind of specimens was that a 1-layer nitrile rubber tape was wrapped inside of the first kind of specimens. The fourth group of the second kind of specimens was internally wrapped with 2-layer nitrile rubber belt, and the outer layer was wrapped with 1-layer, 2-layer, and 3-layer photocurable prepreg tape, respectively.

The specifications of specimen are shown in Table 1. The overlap width of the prepreg tape was 235.5 mm. Both two kinds of specimen should be wound on the expansion device, and the prepreg tap needed to be hardened by ultraviolet illumination radiation for more than 40 minutes. Vaseline was applied to the surface of the expansion device before the specimens were made, then covered with a film to reduce the friction between specimens and the expansion device. Both two kinds of specimens were wound directly on the outer layer of the expansion device without angle. The inner nitrile rubber belt and the outer prepreg tape in the second kind of specimens had staggered lap joints. The nitrile rubber had two sides; one side was smooth and the other side was rough. In this paper, the rough surface of the nitrile rubber belt was used to bond with the prepreg wrap. After the surface was completely hardened, the strain gauges were attached to the corresponding position as shown in Figure 7.

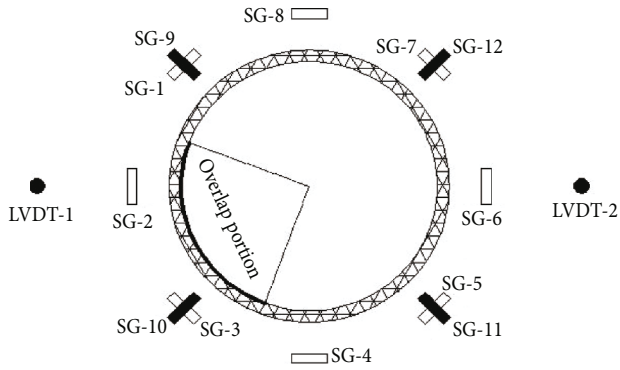

Figure 7: The position of strain gauge and displacement meter.

2.2. Specimen Manufacturing. The specimens were manufactured using the following sequences (Figure 8): (a) the 18 pieces of the middle part of the expansion device were spliced into a cylinder, and both ends were fixed with galvanized iron wire; (b) the steel cover was buckled to two ends of the middle part of the device and fixed with screws and nuts; (c) the device assembled in the first two steps was placed between two benches or cement piers, on which upper angle steel fixed screw was placed; (d) applying Vaseline to the outer surface of the middle device homogeneously, flipping the fixed device manually, and wrapping the tape, rollers were used to remove the bubbles in the specimen to keep the surface smooth and flat, the inner rubber layer of the second specimen could be fixed simply with tape; (e) specimens were placed under a sufficient light source for UV curing, and it was necessary to constantly flip the device so that all parts of the specimen could receive the same amount of ultraviolet radiation and cure homogeneously; (f) after specimens were fully cured (single layer for 15 minutes and double layers for more than 30 minutes under sufficient illumination, multilayer curing was required); marking it in the corresponding position, polishing it smoothly, wiping it clean, and sticking strain gauges; (g) after the strain gauges were stuck to the glue, two steel caps and screws were removed, the device was placed in the middle of the two steel plugs that had been fixed on the universal testing machine, and the contact region between steel plugs and middle part of the device should be smeared with Vaseline for lubrication.

2.3. Auxiliary Device for Expansion

2.3.1. Design of Auxiliary Device for Expansion. There have been some researches on the mechanical properties of FRP-jacketed concrete under vertical compression, mainly on the failure mode and bearing capacity of FRP-jacketed concrete; types of specimens are mainly divided into circular [11–15], rectangular [16–18], square [19], elliptical [20], and other cross-sectional [21] FRP-jacketed concrete columns. Samaan et al. [13] performed axial compression tests on three GFRP-jacketed concrete. Through the analysis of the stress-strain curve, it can be found that the load was

Figure 8: The manufacturing process of the specimen: (a) installing component, (b) wire fixing, (c) lubricating surface, (d) wrapping rubber band, (e) winding prepreg sheet, (f) dislocation overlap, (g) UV curing, (h) applying strain gauge, (i) lubricating surface, and (j) completion.

supported by the concrete in the first half of curve; in the second half of curve, after the concrete was crushed, the load was mainly supported by GFRP tube. This paper will refer to the above research methods to study the mechanical properties of the main cable protection system under the internal circumferential expansion force and design an auxiliary device for expansion [22, 23].

The constitutive relation of confined concrete under compression is fitted according to the experimental data; the constitutive relation of confined concrete under compression is fitted.

During the test, two kinds of specimens were covered outside the middle part, and upper and lower steel disks were inserted into the ends of the auxiliary expansion device. Specimens and the auxiliary expansion device were put into the universal testing machine as a whole. Pressing the plugs at both ends up and down at a certain rate, finally the tapes would crack. The specific dimensions of the auxiliary expansion device are shown in Figure 9.

2.3.2. Force Analysis of Auxiliary Device for Expansion. As shown in Figure 10, the conversion formula of circumferential bearing capacity and the radial displacement can be obtained by calculating longitudinal and transverse force systems of the auxiliary expansion device.

The equation of equilibrium equations of longitudinal force system is

$$F_1 \cos\theta + F_2 \sin\theta = \frac{P}{2\pi R}. \quad (1)$$

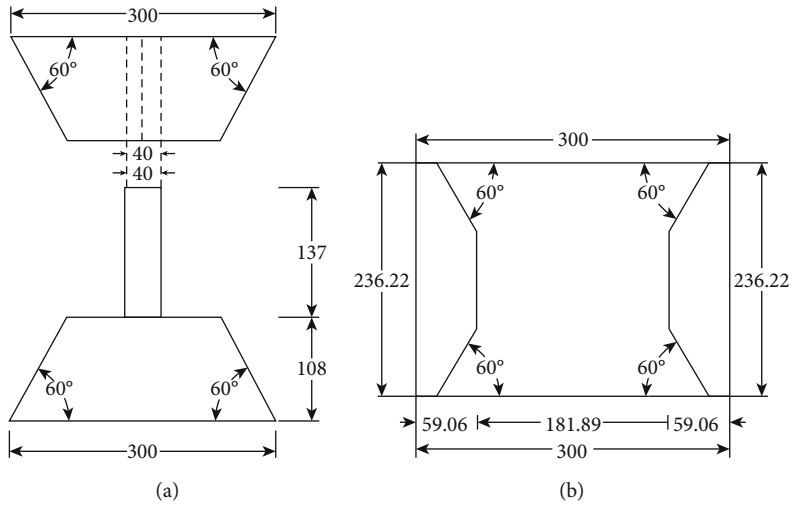

Figure 9: Specific size of the auxiliary expansion device: (a) front view and (b) top view.

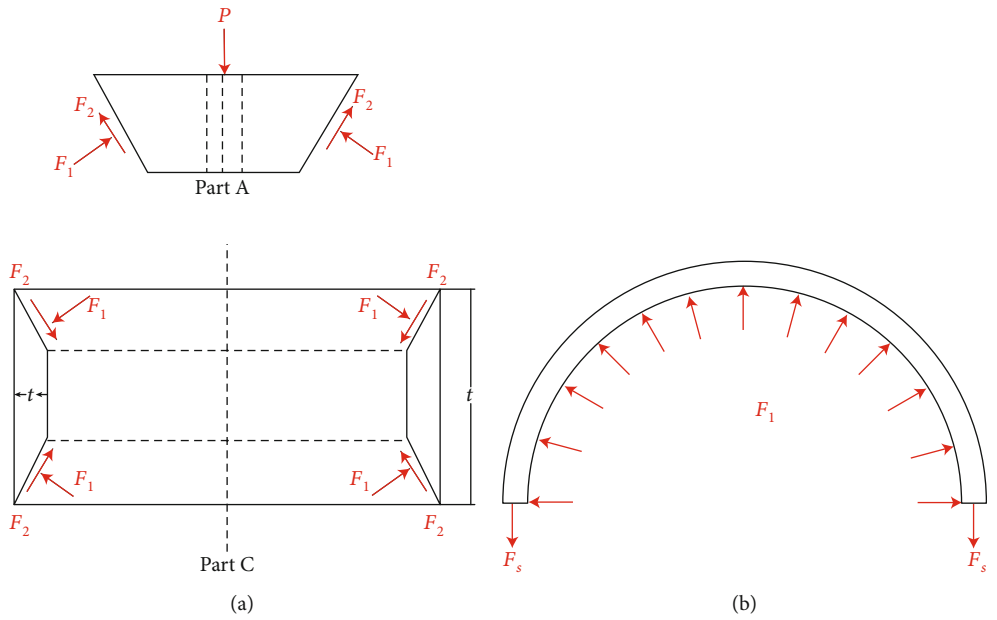

Figure 10: Force analysis of expansion test auxiliary device: (a) force analysis of front view and (b) force analysis of top view.

Supposing the frictional coefficient between A and C is k, $F_2 = F_1 k$,

$$F_1 = \frac{P}{2\pi R(k \sin\theta + \cos\theta)}, \tag{2}$$

$$F_2 = \frac{Pk}{2\pi R(k \sin\theta + \cos\theta)}. \tag{3}$$

In the horizontal direction:

$$F^* = 2(F_1 \sin\theta - F_2 \cos\theta), \tag{4}$$

$$F_s = RF^*. \tag{5}$$

It can be obtained from the specific size of the auxiliary expansion device, $\theta = 60^\circ$, $R = 150$ mm. The frictional coefficient $k = 0.3$ [24] is set here due to the sufficient lubrication between part A and part C and between part C and the specimen. The conversion relationship between the circumferential bearing capacity F and the vertical load P can be obtained by substituting the size of the auxiliary expansion device into equation (4).

$$F = 2\pi R \cdot F^* = 1.885P. \tag{6}$$

The conversion formula of vertical displacement to radial displacement:

$$D_h = \frac{D_v}{\tan\theta}. \tag{7}$$

Substituting the value to equation (7),

$$D_h = 0.577 D_v. \tag{8}$$

According to the solution of the polar coordinate plane of the component under axisymmetric stress, the problem of considering displacement of ring or cylinder under uniform pressure is similar to that under internal pressure of the main cable protection system studied in this paper. Therefore, referring to the above theory, the formula of radial displacement of the main cable protection system can be derived under axisymmetric load.

$$u_\rho = \frac{a^2 q_a (1+\mu)}{E\left(b^2 - a^2\right)} \left[\rho(1-2\mu) - \frac{b^2}{\rho}\right]. \tag{9}$$

The radial displacement value of the main cable protection system can be obtained by substituting the parameters such as inner diameter a, outer diameter b, elastic modulus E, and the Poisson ratio of the specimen into equation (9).

2.4. Experimental Scheme. The test was carried out by using the universal testing machine in Nanjing Tech University, the auxiliary expansion device was used to convert the vertical load of the universal testing machine into a uniform circumferential expansion force, and then, the antiexpansion performance of the composite protection system was tested. The universal testing machine was used with a loading rate of 0.5 mm/min, the accuracy of the universal testing machine could reach up to 0.5 grade, and the loading force could reach up to 600 kN. There were 12 strain gauges on each specimen, 8 in transverse direction and 4 in vertical direction, uniformly arranged along the circumference of the ring of the protection system. In order to compensate for the displacement errors measured by the universal testing machine, two LVDT with a range of 10 cm were installed on the front, back, and two sides of the testing machine to measure the vertical displacement of the testing machine.

The photocurable sheets were cured by a high-power UV curing lamp, and the strain data of the specimen were collected by Static Strain Gauge DN-3816. The experimental phenomena, force, and displacement values should be recorded, so as to analyze the experimental phenomena according to the force-displacement curve. The schematic diagram of the test loading device is shown in Figure 11.

2.5. Experimental Process. In group G-1-X, all three components were wrapped with a layer of photocurable prepreg fiber-reinforced composite tape around the expansion auxiliary device. The loading rate of component G-1-1 was 2 mm/min. The component was destroyed quickly due to the excessive loading rate, and the whole loading process lasted only 85 s. The loading rate of component G-1-2 was adjusted to 0.5 mm/min (the rest of the specimens were all at this rate). In group G-2-X, all three components were wrapped with two layers of photocurable prepreg fiber-reinforced composite tape. The outer two layers of prepreg wrapping tape of the first component were cured simultaneously by continuous wrapping. After curing for 30 minutes, it was found that the thickness of the lap joint was too thick which could not be fully cured. Therefore, the latter two specimens were fabricated by layered wrapping and incremental curing, and each layer was cured for 15 minutes. The following components all adopted this process. In group G-3-X, all three components were wrapped with 3 layers of photocurable prepreg fiber-reinforced composite tape. Specimens were manufactured by layered wrapping and incremental curing, and each layer was cured for 15 minutes. The lap joints of each layer did not coincide with each other. In group G-1-R-X, all three components were wrapped with a layer of nitrile rubber belt and a layer of photocurable prepreg fiber-reinforced composite wrapping tape. In group G-2-R-X, all three components were wrapped with a layer of nitrile rubber belt and 2 layers of photocurable prepreg fiber-reinforced composite wrapping tape. In group G-3-R-X, all three components were wrapped with a layer of nitrile rubber belt and 3 layers of light-cured prepreg fiber-reinforced composite wrapping tape. In group G-X-2R-1, all three components were wrapped with two layers of nitrile rubber belt and then wrapped with one, two, and three layers of light-cured prepreg fiber-reinforced composite wrapping tape, respectively. The time history, maximum circumferential bearing capacity, and radial displacement can be seen in Table 2.

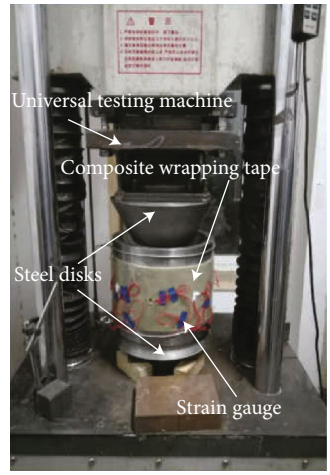

Figure 11: Testing loading device.

3. Experiment Result Analysis

3.1. Failure Modes. Failure modes of the test group without rubber belt are shown in Figure 12. As shown in Figure 12(a), the crack of specimen G-1-X is at the lap joint of prepreg wrapping tape; this specimen broke instantaneously and cracks were vertical. A large number of fibrils were pulled out around it, and no obvious damage was found in other parts. As shown in Figure 12(b), the crack of specimen G-2-X is at the lap joint of the outer prepreg wrapping tape; the specimen broke instantaneously, the broken sound was loud, and the cracks were vertical; a large number of fibrils were pulled out around it. Sounds of fiber breakage were produced during this loading process. As shown in

Table 2: Results of circumferential expansion test.

Specimen	Loading rate (mm (min)-1)	Time history (s)	Maximum circumferential bearing capacity (kN)	Radial displacement (mm)
G-1-X				
G-1-1	2	85	74.18	3.24
G-1-2	0.5	700	57.14	2.47
G-1-3	0.5	912	83.57	3.53
G-2-X				
G-2-1	0.5	750	109.13	2.42
G-2-2	0.5	798	120.46	2.87
G-2-3	0.5	1156	189.54	3.78
G-3-X				
G-3-1	0.5	1414	340.52	5.22
G-3-2	0.5	773	135.41	2.84
G-3-3	0.5	960	216.92	3.33
G-1-R-X				
G-1-R-1	0.5	1392	100.51	4.67
G-1-R-2	0.5	876	75.14	3.22
G-1-R-3	0.5	742	57.34	2.53
G-2-R-X				
G-2-R-1	0.5	926	138.82	3.44
G-2-R-2	0.5	679	140.94	3.43
G-2-R-3	0.5	1148	178.59	4.33
G-3-R-X				
G-3-R-1	0.5	1257	298.94	4.60
G-3-R-2	0.5	1216	278.76	4.35
G-3-R-3	0.5	1200	272.59	4.22
G-X-2R-1				
G-1-2R-1	0.5	791	85.75	3.82
G-2-2R-1	0.5	1127	178.85	4.15
G-3-2R-1	0.5	1333	304.76	4.70

Figure 12(c), the location of cracks in the three layers was not the same, at least one layer destroyed at the lap joint. This specimen broke instantaneously, the sound was loud, and the cracks were vertical; a large number of fibrils were pulled out. Sounds of fiber breakage always occurred during this loading process.

Failure modes of 1-layer rubber belt test group are shown in Figure 13. As shown in Figure 13(a), the crack of specimen G-1-R-X is at the lap joint of the outer prepreg wrapping tape, the specimen broke instantaneously, and cracks were vertical; a small amount of fibrils were pulled out. White vertical cracks appeared during this process and the rubber belt inside was in good condition. As shown in Figure 13(b), the crack of specimen G-2-R-X is at the lap joint of the outer or inner prepreg wrapping tape; the specimen broke instantaneously, the broken sound was loud, and the cracks were vertical. Sounds of fiber breakage and many white vertical cracks were produced during this loading process. The rubber belt was in good condition and bonded well to the prepreg wrapping tape when it was damaged. As shown in Figure 13(c), the cracks of three layers of the two components were all connected, and at least one layer of cracks was in the lap transition position. The specimen broke instantaneously, the broken noise was huge, and the cracks were vertical. Sounds of fiber breakage and white vertical cracks always occurred during this loading process. The rubber belt was in good condition and bonded well to the prepreg wrapping tape when it was damaged.

Failure modes of 2-layer rubber belt test group are shown in Figure 14. As shown in Figure 14(a), the crack of specimen G-1-2R-1 is at the nonlap joint; the specimen broke instantaneously and produced zigzag cracks. White vertical cracks occurred during this loading process. The rubber belt was in good condition. As shown in Figure 14(b), the crack of specimen G-2-2R-1 is at the lap joint of the outer prepreg wrapping tape; the specimen broke instantaneously, broken sound was loud, and outer cracks were vertical. Sounds of fiber breakage and many white vertical cracks were produced during this loading process. The rubber belt was in good condition and bonded well to the prepreg wrapping tape when it was damaged. As shown in Figure 14(c), the cracks of the three layers did not coincide with each other. All of them were not at the lap joint. The specimen broke instantaneously and produced zigzag cracks. Broken noise was huge. Sounds

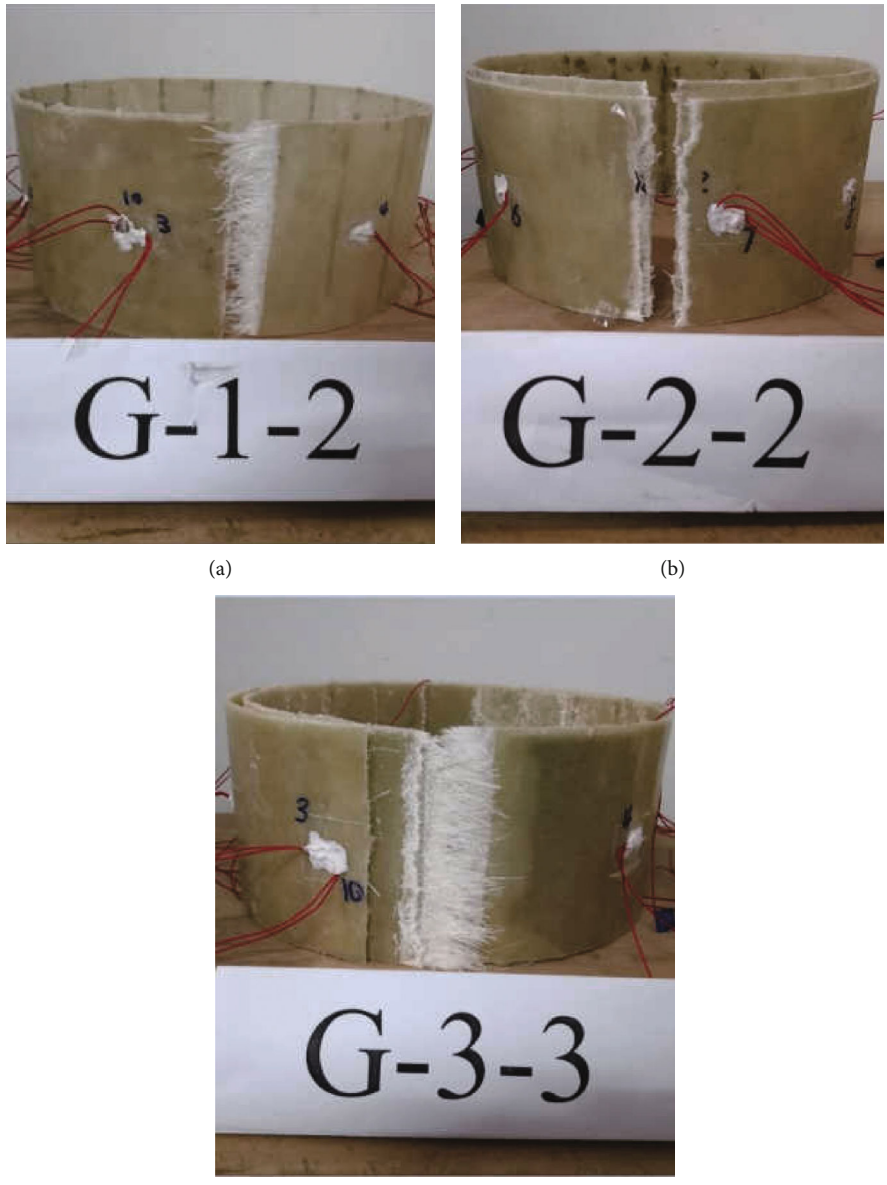

(a) (b)

(c)

Figure 12: Failure modes of the test group without rubber belt.

of fiber breakage and white vertical cracks always occurred during this loading process. The rubber belt was in good condition and bonded well to the prepreg wrapping tape when it was damaged.

3.2. Load-Displacement Curves. Comparisons of circumferential bearing capacity-radial displacement curves of specimens with or without rubber belt are shown in Figure 15. The results of circumferential expansion of the test group without rubber belt are shown in Table 3.

According to the comparable results of the circumferential expansion test between specimens with 2-layer rubber belt and 1-layer rubber belt in Table 4, it can be obtained that when 1-layer prepreg wrap is wrapped around, the circumferential bearing capacity of specimen with 2-layer rubber belt increased by 10.19% and the radial displacement increased by 10.09% compared to the specimen with 1-layer rubber belt; when 2-layer prepreg wrap is wrapped around, the circumferential bearing capacity of specimen with 2-layer rubber belt increased by 3.8% and the radial displacement increased by 11.26% compared to the specimen with 1-layer rubber belt; when 3-layer prepreg wrap is wrapped around the periphery, the circumferential bearing capacity of specimen with 2-layer rubber belt increased by 12.15% and the radial displacement increased by 7.06% compared to the specimen with 1-layer rubber belt. It can be seen that the radial displacement of specimens increases with the increase of rubber belt layers, but the increase rate decreases gradually.

The contribution of the change of layers of the prepreg wrap and rubber belt to the circumferential bearing capacity and the radial displacement of the specimens can be obtained

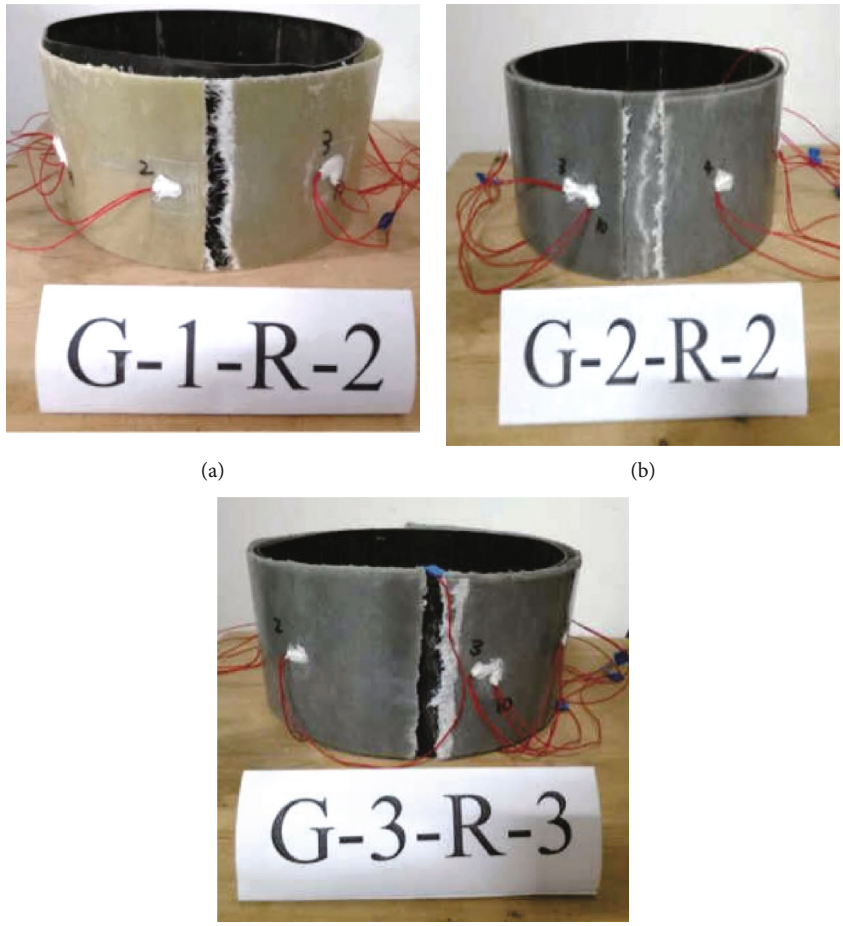

(a) (b)

(c)

Figure 13: Failure modes of 1-layer rubber belt test group.

from Table 5; the change of the number of prepreg layers contributes more to the circumferential bearing capacity than the change of rubber belt layers. When the number of rubber belt layer is the same, the variation of the number of prepreg layers from 1 to 2 on the circumferential bearing capacity is greater than the contribution of the prepreg layers from 2 to 3. The increase of the rubber belt layers also increases the circumferential bearing capacity of the specimen, but there is no obvious regulation to follow. When the number of prepreg layer is the same, the variation of the number of prepreg layers from 2 to 3 on the radial displacement is greater than the contribution of prepreg layers from 1 to 2. However, this trend has gradually declined with the increase of rubber belt. When the number of prepreg layer is the same, the variation of number of rubber belt layers from 0 to 1 is greater than the contribution of the rubber belt layers from 1 to 2, and this trend is most significant when the number of prepreg layer is 2.

3.3. Circumferential Strain-Radial Displacement Curve. This section only selects the circumferential strain-radial displacement curve of representative specimens of each group. The failure modes are analyzed with the change of rubber belt layers under the same number of prepreg layer.

It can be seen from the circumferential strain-radial displacement curve of specimens with 1-layer prepreg wrap from Figure 16 that the closer to the crack position, the greater the strain value is. The strain value of the lap joint of the specimen is the smallest among the all strain gauges. There is also a phenomenon in which the strain of nondestructive position suddenly increases during the loading process. It is suggested that this is mainly caused by instant stretching of the internal fiber fold or the fracture of the internal fiber fabric. The radial displacement of the component is 2.44 mm without rubber belt, 2.58 mm for 1-layer rubber belt, and 2.72 mm for 2-layer rubber belt when the failure strain of the component reaches 95%. As the number of rubber belt layers increases, the radial displacement of components becomes larger when they are damaged.

It can be seen from the circumferential strain-radial displacement curve of specimens with 2-layer prepreg wrap from Figure 17 that the strain values of components are small at the initial stage of loading, which is caused by the compaction of components of the loading device. When the layers of external prepreg wrap increases to 2, the radial displacement becomes larger as the number of rubber belt increases. The radial displacement of the component is 2.31 mm without rubber belt, 3.28 mm for 1-layer rubber belt, and 3.95 mm

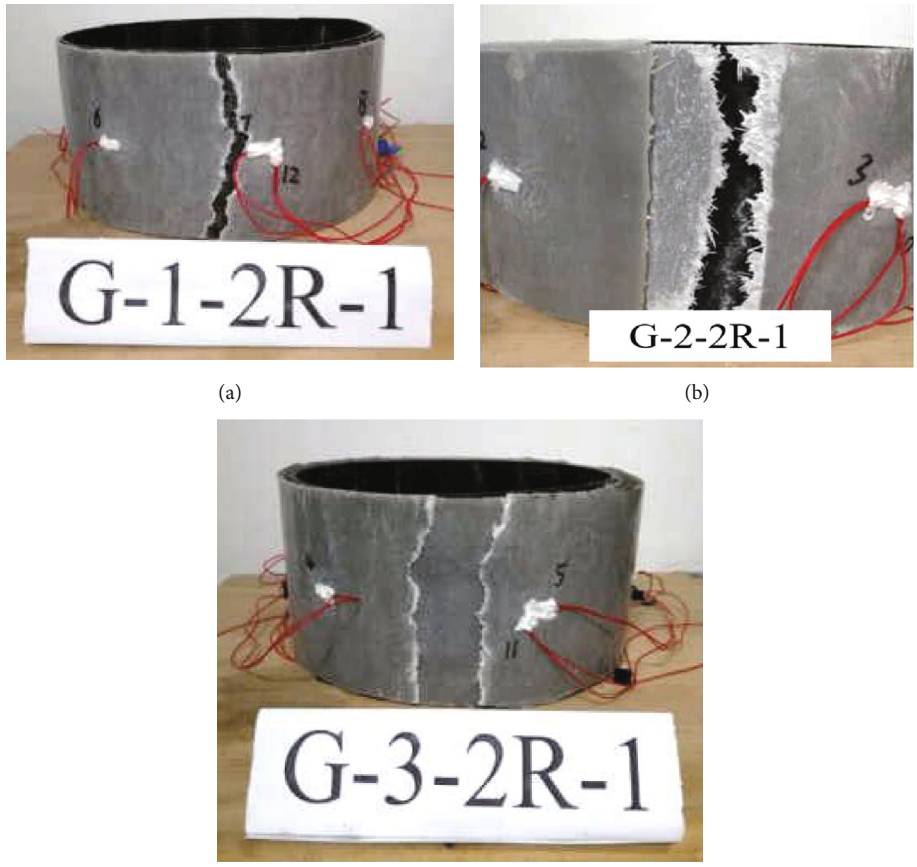

(a) (b)

(c)

Figure 14: Failure modes of 2-layer rubber belt test group.

for 2-layer rubber belt when the failure strain of 2-layer prepreg wrap reaches 95%. The strain value of the specimen close to the failure position is the largest, and the value of the overlap portion is smaller.

It can be seen from the circumferential strain-radial displacement curve of specimens with 3-layer prepreg wrap from Figure 18 that the strain values of components are small at the initial stage of loading, which is caused by the compaction of components of the loading device. The value at most locations during the loading process increases substantially linearly. Similar to the former two groups, the increase in the number of rubber belt layer significantly affects the radial displacement of the specimen when they are broken. As the number of rubber belt layer increases, the radial displacement of the component is 3.18 mm without rubber belt, 4.04 mm for 1-layer rubber belt, and 4.51 mm for 2-layer rubber tape when the failure strain of the component reaches 95%. Similar to the previous two groups, the strain value of the specimen close to the failure position is the largest, and the strain value of the overlap portion is smaller.

4. Expansion Force of the Main Cable

In this paper, the main research direction of the main cable protection system of new suspension bridge is to resist the expansion performance of the main cable affected by temperature. Therefore, this section begins with the expansion of the main cable, focusing on the expansion of the main cable in plane. The temperature stress of the main cable can be obtained according to the following:

$$\varepsilon_t = \Delta t \cdot \alpha = \frac{\sigma_t}{E}. \tag{10}$$

Δt is the maximum temperature difference of the environment, α is the linear expansion coefficient of the main cable, E is the elastic modulus of steel wire for the main cable, σ_t is the temperature stress of the main cable, and ε_t is the temperature strain of the main cable.

The temperature stress of the main cable can be calculated as follows:

$$\sigma_t = \Delta t \cdot \alpha \cdot E. \tag{11}$$

Aiming at the expansion of the main cables in plane affected by temperature, the expansive force along the circumferential direction of the main cable mainly focused on the ring of the protective system of unit thickness, so the value of A and expansion force of the main cable protection

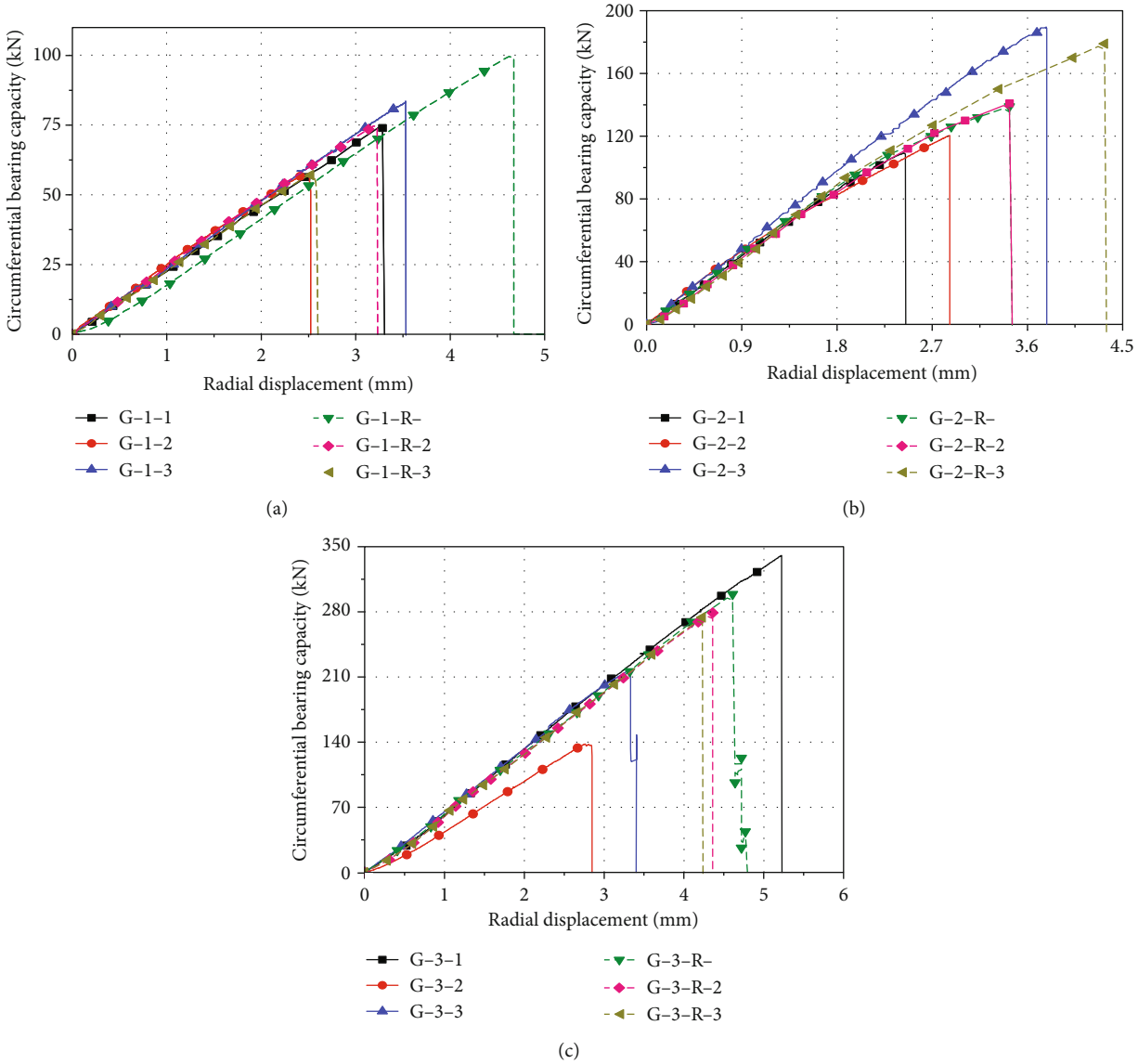

Figure 15: Comparison of circumferential bearing capacity-radial displacement curves of specimens with or without rubber belt: (a) 1-layer prepreg component, (b) 2-layer prepreg component, and (c) 3-layer prepreg component.

Table 3: Results of circumferential expansion test of the test group without rubber belt.

Group	Specimen	Circumferential bearing capacity (kN)	Average (kN)	Radial displacement (mm)	Average (mm)
G-1-X	G-1-1	74.18	71.63	3.24	3.08
	G-1-2	57.14		2.47	
	G-1-3	83.57		3.53	
G-2-X	G-2-1	109.13	139.71	2.42	3.02
	G-2-2	120.46		2.87	
	G-2-3	189.54		3.78	
G-3-X	G-3-1	340.52	230.95	5.22	3.80
	G-3-2	135.41		2.84	
	G-3-3	216.92		3.33	

Table 4: Results of circumferential expansion test of rubber belt test group.

Group	Specimen	Circumferential bearing capacity (kN)	Average (kN)	Radial displacement (mm)	Average (mm)
G-1-R-X	G-1-R-1	100.51	77.66	4.67	3.47
	G-1-R-2	75.14		3.22	
	G-1-R-3	57.34		2.53	
G-1-2R-1	G-1-2R-1	—	85.57	—	3.82
G-2-R-X	G-2-R-1	138.82	152.78	3.44	3.73
	G-2-R-2	140.94		3.43	
	G-2-R-3	178.59		4.33	
G-2-2R-1	G-2-2R-1	—	178.85	—	4.15
G-3-R-X	G-3-R-1	298.94	283.43	4.60	4.39
	G-3-R-2	278.76		4.35	
	G-3-R-3	272.59		4.22	
G-3-2R-1	G-3-2R-1	—	304.76	—	4.70

Table 5: The influence of the number of the prepreg wrap and rubber belt layers on the circumferential bearing capacity and radial displacement of the specimen.

	Number of rubber layer	Number of prepreg layer ($1 \rightarrow 2$)	Number of prepreg layer ($2 \rightarrow 3$)	Number of prepreg layer	Number of rubber belt layer ($0 \rightarrow 1$)	Number of rubber belt layer ($1 \rightarrow 2$)
Growth rate of radial displacement	0	-1.95%	25.83%	1	12.66%	10.09%
	1	7.49%	17.69%	2	23.51%	11.26%
	2	8.64%	13.25%	3	15.53%	7.06%
Growth rate of circumferential bearing capacity	0	95.04%	65.31%	1	8.42%	10.19%
	1	96.73%	85.52%	2	9.36%	17.64%
	2	109.01%	70.4%	3	22.72%	7.53%

system affected by temperature F_r can be calculated by the following:

$$\begin{aligned} A &= \pi D, \\ F_r &= \sigma_t \cdot A. \end{aligned} \tag{12}$$

Therefore, the linear expansive force of the main cable cross section is $(\pi D \cdot \Delta t \cdot \alpha \cdot E)$ kN.

According to the force balance on the compressive performance of CFRP sheath confined concrete [25], the relationship between confined sheath stress and circumferential stress can be obtained, which can be used to calculate the confined stress circumferential tensile stress of FRP sheath confined to the main cable. The diagram of restrained and circumferential stress of FRP sheath is shown in Figure 19.

$$f_r = -\frac{2t_j}{D} f_{j\theta}. \tag{13}$$

f_r is the constrained stress, $f_{j\theta}$ is the circumferential stress, t_j is the thickness of FRP sheath, and D is the diameter of the main cable.

When the temperature difference reaches Δt, the stress produced by the main cable under temperature load $\sigma_t = f_r = \Delta t \cdot \alpha \cdot E$. So the circumferential stress can be obtained from the following:

$$f_{j\theta} = \left| -\frac{f_r \cdot D}{2t_j} \right|. \tag{14}$$

When the tensile strength of the prepreg sheet measured by the material characteristic test is less than the circumferential stress $f_{j\theta}$, the use of prepreg wrapping tape alone cannot meet the requirements of the protection system. The energy of main cable deformation is absorbed by the deformation of rubber belt, so as to reduce the force on the FRP wrapping tape.

The linear expansion coefficient of the main cable is used to calculate the cross-sectional deformation of the main cable:

$$\varepsilon_R = \frac{R_t - R_0}{R_0} = \alpha \cdot \Delta t. \tag{15}$$

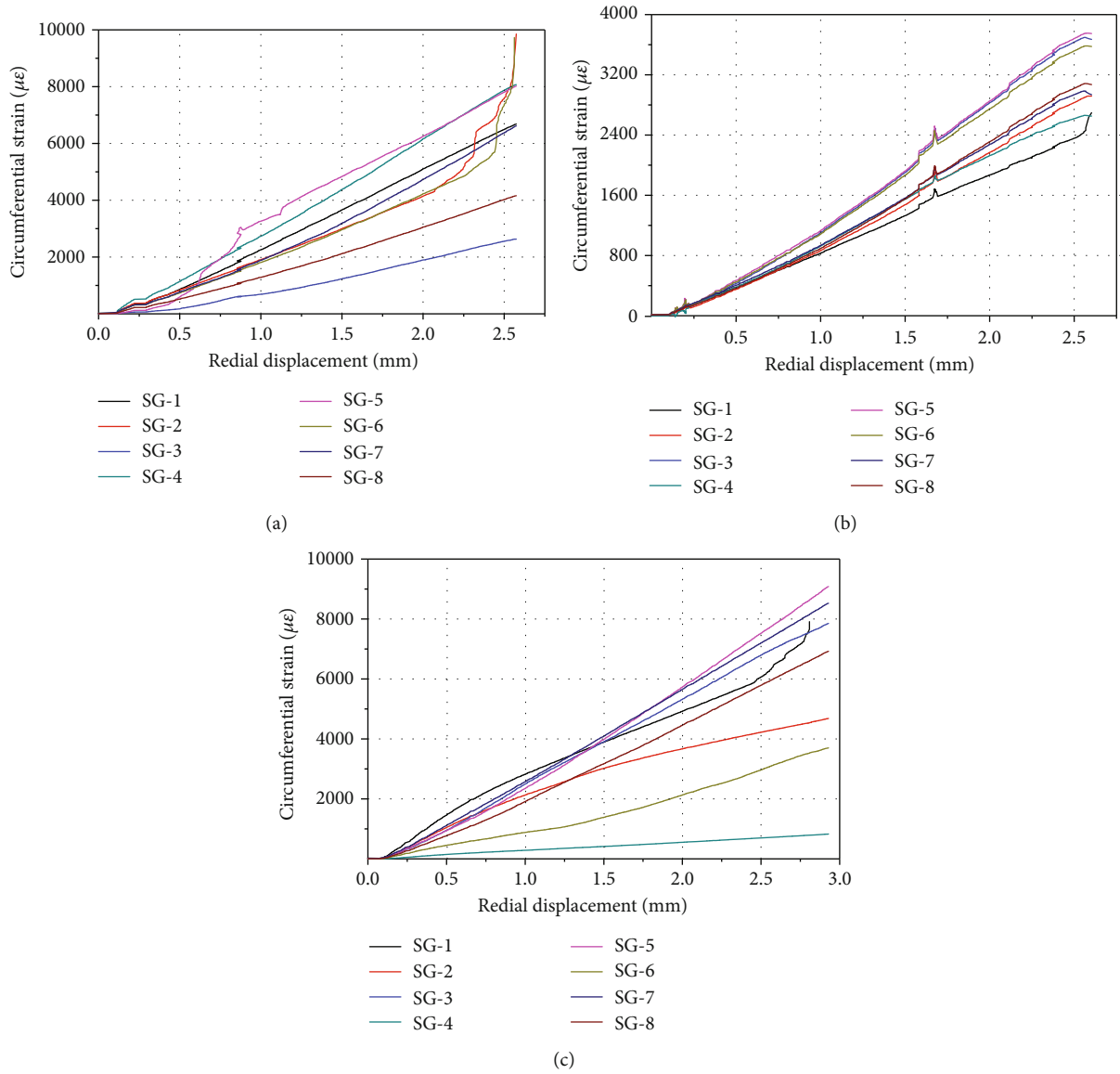

Figure 16: The circumferential strain-radial displacement curve of the test group with 1-layer prepreg wrap: (a) G-1-2 curve, (b) G-1-R-3 curve, and (c) G-1-2R-1 curve.

ε_R is the radius strain of the main cable cross section, R_t is the radius of the main cable after expansion, and R_0 is the radius of the main cable before expansion.

Querying the related parameters, the linear expansion coefficient of the main cable is $1.2 \times 10^{-5}/^{\circ}\mathrm{C}$, and the maximum temperature difference is 60°C.

$$\Delta R = \alpha \cdot \Delta t \cdot R_0. \tag{16}$$

The radius difference of the main cable before and after expansion is 0.108 mm. In addition to temperature deformation, the main cable will also be deformed by the sloshing and vibration of the main cable; the use of rubber belt can play a role in shock absorption. According to the expansion test of the main cable, the radial displacement of 1, 2, and 3 layers of prepreg wrap protection system increases by 0.39 mm, 0.71 mm, and 0.59 mm, respectively, when the rubber belt layer increases from 0 to 1. It can be seen that when the outer prepreg layer is 2, the radial displacement increment of the inner rubber belt is the largest, and the increment is also greater than the main cable deformation 0.108 mm, which can meet the deformation requirements of the main cable.

5. Conclusions

In this paper, the circumferential expansion test of the composite wrap system for main cable protection of new suspension bridge is studied. The failure modes of the protective system of different prepreg wraps and with or without rubber belts are compared. Based on theoretical analysis, the theoretical values of the circumferential bearing capacity and radial displacement of specimen under the action of

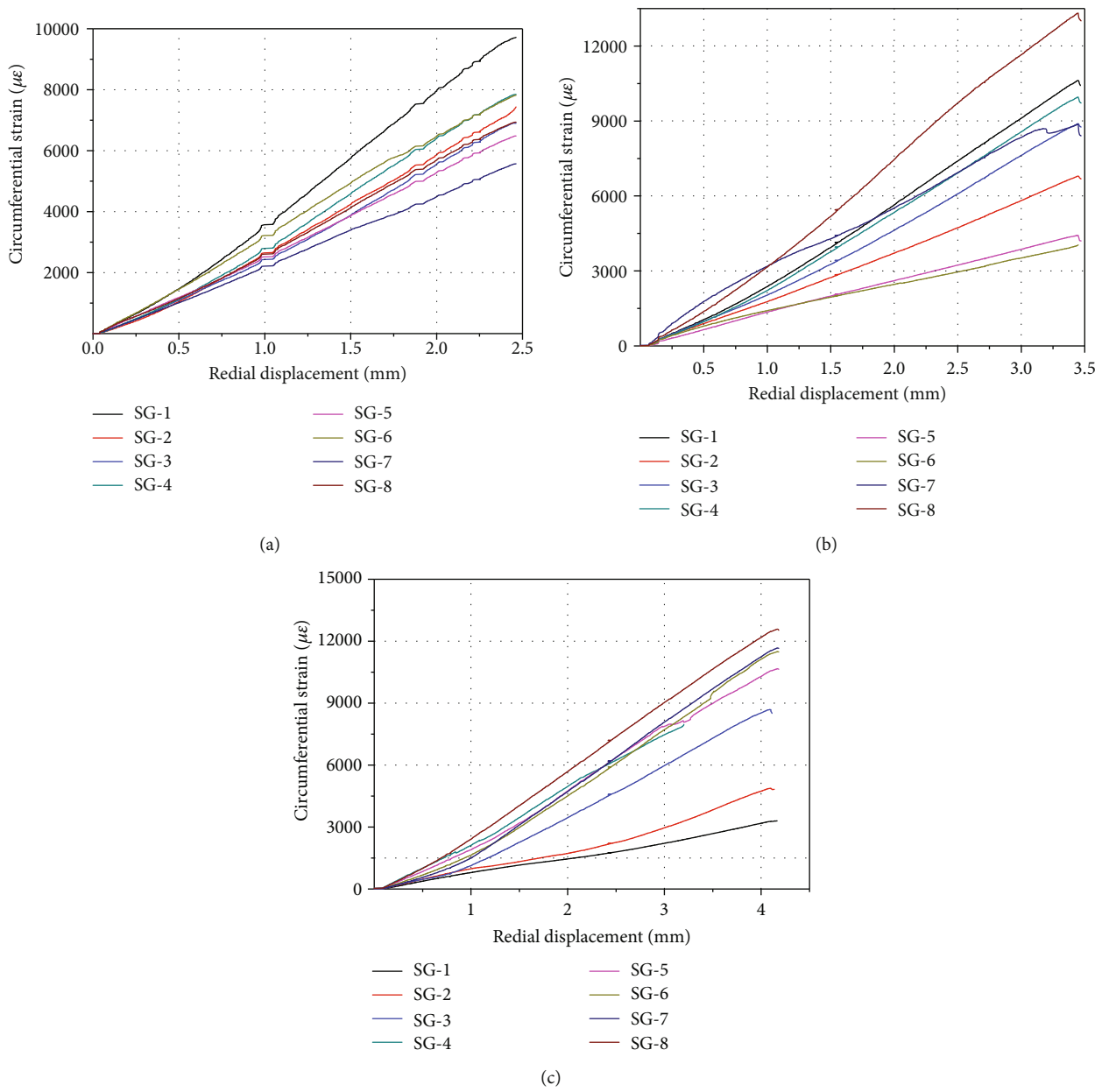

Figure 17: The circumferential strain-radial displacement curve of the test group with 2-layer prepreg wrap: (a) G-2-1 curve, (b) G-2-R-1 curve, and (c) G-2-2R-1 curve.

circumferential expansion force are derived. The corresponding major conclusions are summarized as follows:

(1) An experiment scheme for circumferential expansion of the main cable protection system is designed. The failure modes of components with different prepreg wrap layers and rubber belt layers were compared and analyzed. The radial displacement of the component is the most obviously affected by the increase of rubber belt layers. When the rubber belt layer is added, the deformation of the main cable is increased and the component has more deformation redundancy, which delays the ultimate strain of the outer prepreg wrap. The entire system can be better deformed following the deformation of the main cable

(2) The change of the number of prepreg wrap layers contributes more to the circumferential capacity. When the number of rubber belt layers is the same, with the increase of prepreg layers, the growth rate of circumferential bearing capacity decreases gradually; conversely, the growth rate of radial displacement increases gradually. When the number of prepreg layers is 2 and the number of rubber belt layers is 1, the growth rates of radial displacement and circumferential bearing capacity are maximal

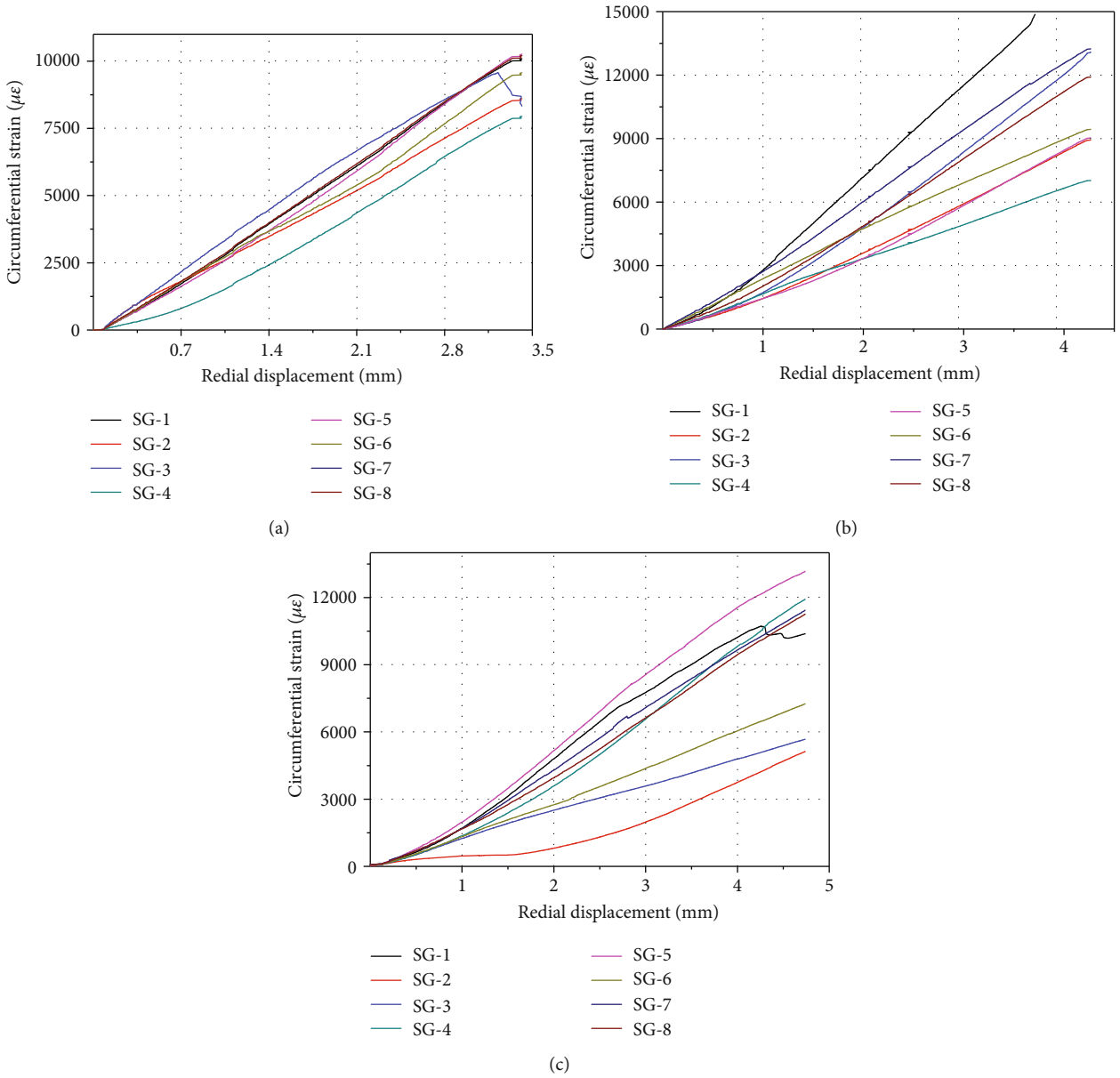

Figure 18: The circumferential strain-radial displacement curve of the test group with 3-layer prepreg wrap: (a) G-3-3 curve, (b) G-3-R-3 curve, and (c) G-3-2R-1 curve.

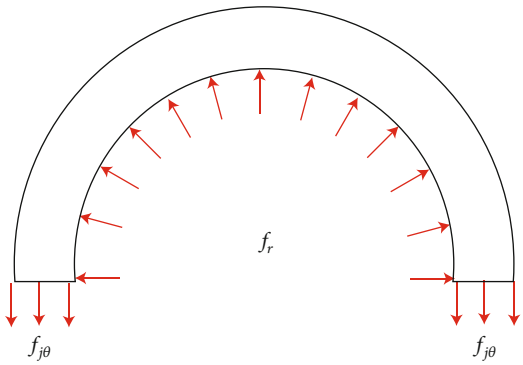

Figure 19: Restrained stress and circumferential stress of FRP sheath.

(3) At the initial stage of loading, the strain values of components are small; the value at most locations during the loading process increases substantially linearly. The strain value of the specimen close to the failure position is the largest, and the value of the overlap portion is smaller

(4) When the tensile strength of the prepreg sheet measured by the material characteristic test is less than the circumferential stress $f_{j\theta}$, the use of prepreg wrapping tape alone cannot meet the requirements of the protection system. When the rubber belt is introduced, the component has more redundant deformation, which delays the arrival of limit strain of the outer prepreg wrapping tape, and makes the

whole system better follow the deformation of the main cable

Data Availability

The data used to support the findings of this study are available from the corresponding author upon request.

Conflicts of Interest

The authors declare that they have no conflicts of interest.

Acknowledgments

The research described here was supported by the National Natural Science Foundation of China (Grant No. 51778285), the Natural Science Foundation for Distinguished Young Scholars of Jiangsu Province (Grant No. BK20190034), the National Key Research and Development Program of China (2019YFD1101205), and the Funds for Youth Creative Research Groups of Nanjing Tech University.

References

[1] H. Q. Zhao, X. J. He, M. Zhao, and J. W. Zhao, "On the development and innovation of modern suspension bridge in China," *Applied Mechanics and Materials*, vol. 587-589, pp. 1435–1438, 2014.

[2] M. R. T. Arruda and J. P. M. Serafim, "Parametric test for the preliminary design of suspension bridges," *International Journal of Advanced Structural Engineering*, vol. 9, no. 2, article 156, pp. 165–176, 2017.

[3] A. Juozapaitis, S. Idnurm, G. Kaklauskas, J. Idnurm, and V. Gribniak, "Non-linear analysis of suspension bridges with flexible and rigid cables," *Journal of Civil Engineering and Management*, vol. 16, no. 1, pp. 149–154, 2010.

[4] T. L. M. Morgado and A. Sousa e Brito, "A failure analysis study of a prestressed steel cable of a suspension bridge," *Case Studies in Construction Materials*, vol. 3, pp. 40–47, 2015.

[5] J. A. Roebling, *Columbia Electronic Encyclopedia*, Columbia University Press, New York, 6th edition, 2019.

[6] T. Tarui, S. Konno, and T. Takahashi, "High strength galvanized wire for bridge cables," *Materials Science Forum*, vol. 426-432, pp. 829–834, 2003.

[7] T. Kitada, "Considerations on recent trends in, and future prospects of, steel bridge construction in Japan," *Journal of Constructional Steel Research*, vol. 62, no. 11, pp. 1192–1198, 2006.

[8] M. L. Bloomstine, O. Sørensen, and J. V. Thomsen, "Main cable corrosion protection by dehumidification," *IABSE Symposium Report*, vol. 91, no. 2, pp. 1–8, 2006.

[9] H. Petroski, "Akashi Kaikyo Bridge," *American Scientist*, vol. 97, no. 3, pp. 192–196, 2009.

[10] H. Fang, Y. Bai, W. Liu, Y. Qi, and J. Wang, "Connections and structural applications of fibre reinforced polymer composites for civil infrastructure in aggressive environments," *Composites Part B: Engineering*, vol. 164, pp. 129–143, 2019.

[11] A. Nanni and N. M. Bradford, "FRP jacketed concrete under uniaxial compression," *Construction and Building Materials*, vol. 9, no. 2, pp. 115–124, 1995.

[12] A. Mirmiran and M. Shahawy, "Behavior of concrete columns confined by fiber composites," *Journal of Structural Engineering*, vol. 123, no. 5, pp. 583–590, 1997.

[13] M. Samaan, A. Mirmiran, and M. Shahawy, "Model of concrete confined by fiber composites," *Journal of Structural Engineering*, vol. 124, no. 9, pp. 1025–1031, 1998.

[14] G. Lin, T. Yu, and J. G. Teng, "Design-oriented stress–strain model for concrete under combined FRP-steel confinement," *Journal of Composites for Construction*, vol. 20, no. 4, article 04015084, 2016.

[15] H. M. Elsanadedy, Y. A. Al-Salloum, S. H. Alsayed, and R. A. Iqbal, "Experimental and numerical investigation of size effects in FRP-wrapped concrete columns," *Construction and Building Materials*, vol. 29, pp. 56–72, 2012.

[16] P. Rochette and P. Labossière, "Axial testing of rectangular column models confined with composites," *Journal of Composites for Construction*, vol. 4, no. 3, pp. 129–136, 2000.

[17] H. Toutanji, M. Han, J. Gilbert, and S. Matthys, "Behavior of large-scale rectangular columns confined with FRP composites," *Journal of Composites for Construction*, vol. 14, no. 1, pp. 62–71, 2010.

[18] P. Sadeghian, A. R. Rahai, and M. R. Ehsani, "Experimental study of rectangular RC columns strengthened with CFRP composites under eccentric loading," *Journal of Composites for Construction*, vol. 14, no. 4, pp. 443–450, 2010.

[19] M. A. G. Silva, "Behavior of square and circular columns strengthened with aramidic or carbon fibers," *Construction and Building Materials*, vol. 25, no. 8, pp. 3222–3228, 2011.

[20] J. G. Teng and L. Lam, "Compressive behavior of carbon fiber reinforced polymer-confined concrete in elliptical columns," *Journal of Structural Engineering*, vol. 128, no. 12, pp. 1535–1543, 2002.

[21] P. Feng, S. Cheng, Y. Bai, and L. Ye, "Mechanical behavior of concrete-filled square steel tube with FRP-confined concrete core subjected to axial compression," *Composite Structures*, vol. 123, pp. 312–324, 2015.

[22] T. Yu, B. Zhang, and J. G. Teng, "Unified cyclic stress–strain model for normal and high strength concrete confined with FRP," *Engineering Structures*, vol. 102, pp. 189–201, 2015.

[23] Y. M. Hu, T. Yu, and J. G. Teng, "FRP-confined circular concrete-filled thin steel tubes under axial compression," *Journal of Composites for Construction*, vol. 15, no. 5, pp. 850–860, 2011.

[24] K. Shimizu, T. Noguchi, H. Seitoh, and E. Muranaka, "FEM analysis of the dependency on impact angle during erosive wear," *Wear*, vol. 233-235, pp. 157–159, 1999.

[25] Y. Xiao and H. Wu, "Compressive behavior of concrete confined by carbon fiber composite jackets," *Journal of Materials in Civil Engineering*, vol. 12, no. 2, pp. 139–146, 2002.